1-1-2007

Averaging of the Electron Effective Mass in Multicomponent Transparent Conducting Oxides

Julia E. Medvedeva
Missouri University of Science and Technology, juliaem@mst.edu

A Letters Journal Exploring the Frontiers of Physics

June 2007

EPL, **78** (2007) 57004
doi: 10.1209/0295-5075/78/57004

www.epljournal.org

Averaging of the electron effective mass in multicomponent transparent conducting oxides

J. E. Medvedeva

Department of Physics, University of Missouri-Rolla - Rolla, MO 65409, USA

received 16 January 2007; accepted in final form 23 April 2007
published online 21 May 2007

PACS 71.20.-b – Electron density of states and band structure of crystalline solids

Abstract – We find that layered materials composed of various oxides of cations with s^2 electronic configuration, XY_2O_4, X = In or Sc, Y = Ga, Zn, Al, Cd and/or Mg, exhibit isotropic electron effective mass which can be obtained via averaging over those of the corresponding single-cation oxide constituents. This effect is due to a hybrid nature of the conduction band formed from the *s*-states of *all* cations and the oxygen *p*-states. Moreover, the observed insensitivity of the electron effective mass to the oxygen coordination and to the distortions in the cation-oxygen chains suggests that a similar behavior can be expected in the technologically important amorphous state. These findings significantly broaden the range of materials as efficient transparent conductor hosts.

Transparent conducting oxides (TCOs) —the vital part of many optoelectronic devices— have been known for a century and employed technologically for decades [1–5]. Yet, the current TCO market is dominated by only three materials, In_2O_3, SnO_2 and ZnO, and the research efforts are primarily focused on the oxides of post-transition metals with $(n-1)d^{10}ns^2$ electronic configuration. Despite excellent optical and thermal properties as well as low cost, oxides of the main group metals, such as Al_2O_3, SiO_2, MgO and CaO, have never been considered as candidates to achieve useful electrical conductivity due to the challenges of efficient carrier generation in these wide-bandgap materials [6–8].

Multicomponent TCO with layered structure, *e.g.*, $InGaZnO_4$ [9–14], drew attention due to a possibility to separate carrier donors (traditionally, oxygen vacancies or aliovalent substitutional dopants) and the conducting layers where carriers are transfered without charge scattering on the impurities. In $InGaZnO_4$, octahedrally coordinated In layers alternate with double layers of oxygen tetrahedrons around Ga and Zn, fig. 1. Because octahedral oxygen coordination of cations was long believed to be essential for a good transparent conductor [9,15–18], it has been suggested that in $InGaZnO_4$ the charge is transfered within the $InO_{1.5}$ layers while the atoms in $GaZnO_{2.5}$ layers were proposed as candidates for efficient doping [9–11]. Conversely, it has been argued that $InGaO_3(ZnO)_m$ is a Zn 4*s* conductor [12].

To understand the role of local symmetry in the intrinsic transport properties of TCOs and to determine the functionality of structurally and chemically distinct layers in $InGaZnO_4$, we employ the *ab initio* density functional approach to study the electronic properties of various single and multi-cation oxides. Further, using $InGaZnO_4$ as a test model which exemplifies not only the structural

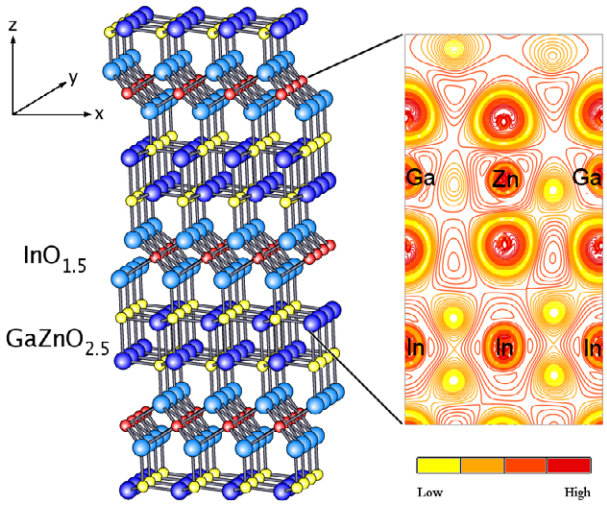

Fig. 1: (Colour online) The unit cell of $InGaZnO_4$ where three similar blocks consisting of one $InO_{1.5}$ and two $GaZnO_{2.5}$ alternate along the [0001] direction. Ga and Zn atoms are distributed randomly. Three-dimensional *interatomic* (background) charge density distribution is evident from the contour plot calculated in the (011)-plane. The plotted charge density corresponds to the carrier concentration of $\sim 1 \times 10^{18}$ cm^{-3}.

Table 1: Net contributions from the states of the atoms that belong to the X-O1 or Y_2-O2 layers (X = In or Sc, Y = Ga, Zn, Al, Cd and/or Mg) to the conduction band wave function at the Γ point, in per cent; and the electron effective masses m, in m_e, calculated from the band structure of the layered oxides and the components of the electron effective-mass tensor, $m_{a,b}$, and m_z, calculated from eqs. (1) and (2) using the effective masses of the corresponding single-cation oxides.

XY_2O_4	N_X	N_{O1}	N_{Y_2}	N_{O2}	$m_{[100]}$	$m_{[010]}$	$m_{[001]}$	m_{ab}	m_z
$InGaZnO_4$	23	25	29	23	0.23	0.22	0.20	0.23	0.23
$InAlCdO_4$	27	27	18	28	0.26	0.25	0.20	0.27	0.27
$InGaMgO_4$	27	31	21	21	0.27	0.27	0.24	0.28	0.29
$InAlMgO_4$	33	40	12	15	0.32	0.31	0.35	0.31	0.34
$ScGaZnO_4$	8	19	40	33	0.33	0.33	0.34	0.33	0.53

but also the combinatorial peculiarities of complex TCOs, we survey other ns^2 cations —beyond the traditional In, Zn and Ga— for a possibility of being effectively incorporated into novel multicomponent TCO hosts.

Isotropy of the electronic properties in $InGaZnO_4$. – The electronic band structure calculations for $InGaZnO_4$ show that the atoms from both $InO_{1.5}$ and $GaZnO_{2.5}$ layers give comparable contributions to the conduction band, fig. 2, leading to a three-dimensional distribution of the charge density, fig. 1. Moreover, the isotropy of the electronic properties in this layered material manifests itself in the electron effective masses being nearly the same in all crystallographic directions (table 1).

The conduction band in $InGaZnO_4$ consists of a set of highly dispersed parabolic bands, fig. 3(a). Since the band gap values in the corresponding single-metal oxides are different, one may expect that each band is attributed to a certain cation in this multicomponent compound. However, we find that each band cannot be assigned to a state of a particular atom since all atoms in the cell, including the oxygen atoms, give non-negligible contributions to the conduction band wave function, fig. 2 and table 1.

The conduction band dispersion calculated along the [0001] crystallographic direction for a *single* unit cell, fig. 3(b), reveals that the multiple bands can be attributed to a "folding" of one parent band. Triple unfolding of the conduction band corresponds to the three-time reduction (expansion) of the conventional unit cell (Brillouin zone) in the z-direction. Since the block of three layers (one $InO_{1.5}$ and two $GaZnO_{2.5}$ layers, fig. 1) is repeated in the unit cell via translation, the splitting between the resulting bands (for the k-vector equal to $\frac{\pi}{c}$, $\frac{2\pi}{c}$, $\frac{4\pi}{c}$, ..., fig. 3(c)) is negligible. Although the subsequent unfolding into three individual layers is not justified because the three layers are structurally and chemically dissimilar, fig. 1, we find that the band can be unfolded again, fig. 3(c). The resulting highly dispersed band is in accord with the stepless increase of the density of states, fig. 3(d). Thus, the conduction band can be "unfolded" nine times that corresponds to the total number of layers in the unit cell. Therefore, the electronic properties of the individual layers are similar.

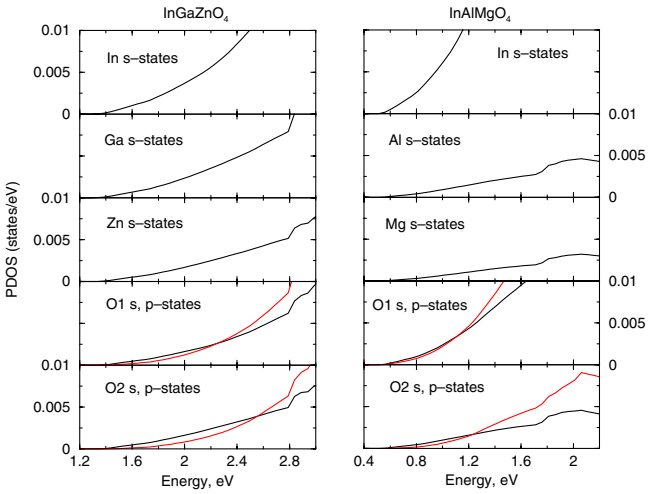

Fig. 2: (Colour online) Partial density of states at the bottom of the conduction band for $InGaZnO_4$ and $InAlMgO_4$. Atoms from both In-O1 and Ga-Zn-O2 (or Al-Mg-O2) layers give non-negligible contributions.

Unconventional s^2-cations at work. – A two-dimensional electronic structure could be expected in $InAlMgO_4$ and $ScGaZnO_4$ since the band gap values in Sc_2O_3, Al_2O_3 and MgO are at least twice larger than those in In_2O_3, Ga_2O_3, CdO and ZnO and, hence, the unoccupied s-states of Sc, Al and Mg should be located deeper in the conduction band. From the analysis of the partial density of states for $InGaMgO_4$, $InAlCdO_4$, $ScGaZnO_4$ and $InAlMgO_4$, we find that although the contributions to the bottom of the conduction band from Sc, Al and Mg atoms are notably reduced, these states are available for electron transport, fig. 2. Thus, similar to $InGaZnO_4$ where the cations s-states are energetically compatible, in all multicomponent oxides considered, the conduction band wave function is a combination of the s-states of *all* cations and the p-states of the oxygen atoms. The contributions from the chemically distinct layers are comparable, table 1, and, consequently, these complex oxides exhibit a three-dimensional network for the electron transport and isotropic electron effective mass, table 1.

Comparison to single-cation TCOs. – The unfolded conduction band in the layered multicomponent

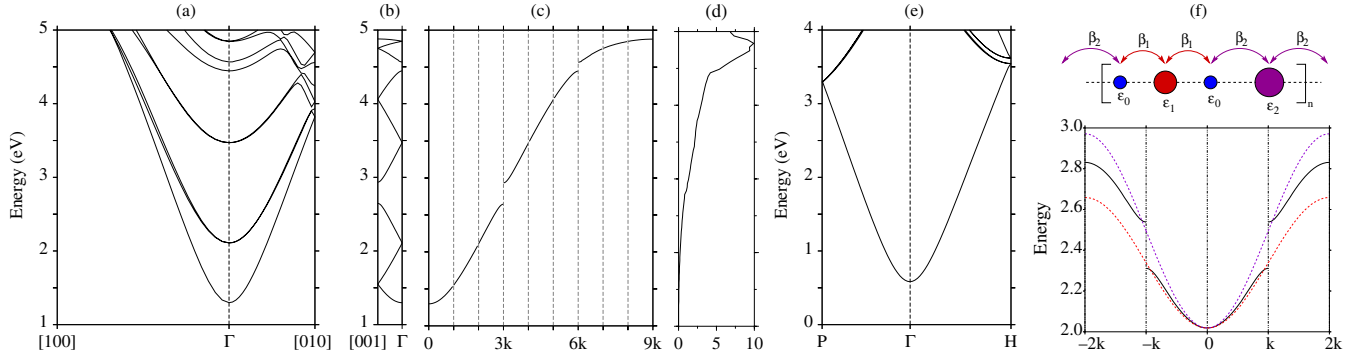

Fig. 3: (Colour online) Electronic band structure of single- and multi-cation oxides. (a) Conduction band dispersion calculated in the *ab*-plane and (b) along the [0001] direction in $InGaZnO_4$. (c) The conduction band unfolded nine times that corresponds to the number of [0001] layers in the unit cell, $k = \frac{\pi}{c}$, c is the lattice parameter. The resulting single free-electron-like band is in accord with the stepless total density of states (d), in states/eV. (e) Conduction band of In_2O_3 is given for comparison. (f) Tight-binding conduction band (solid line) calculated for one-dimensional atomic chain depicted above the plot. Two types of metal atoms (red and purple spheres) alternate with oxygen atoms (blue spheres) and only the nearest-neighbor hopping β is assumed. To illustrate the effective mass averaging, cf. eq. (1), the conduction bands for the corresponding single-metal oxide chains (dashed lines) are aligned with $(\varepsilon_1 + \varepsilon_2)/2$.

materials resembles those of single-cation TCOs, *e.g.*, In_2O_3, cf. figs. 3(c) and (e). Such a highly dispersed single conduction band is the key attribute of any conventional [19] *n*-type TCO host [9,17,20–24]. Upon proper doping, it provides both high mobility of extra carriers (electrons) due to their small effective mass, and low optical absorption due to high-energy inter-band transitions from the valence band, E_v, and from the partially filled conduction band, E_c, fig. 4. Even in relatively small-bandgap oxides, *e.g.*, CdO where the optical band gap, E_g, is 2.3 eV, the high energy dispersion ensures a pronounced Fermi energy displacement with doping (the so-called Burstein-Moss shift) which helps to keep the intense transitions from the valence band out of the visible range. However, the large carrier concentrations required for good electrical conductivity may result in an increase of the optical absorption due to low-energy transitions from the Fermi level up into the conduction band as well as plasma frequency. Application-specific optical properties and desired band offsets (work functions) can be attained in a multicomponent transparent conductor with a proper composition.

In both single- and multi-cation oxides, the conduction band is formed from the empty *s*-states of the metal atoms and the oxygen antibonding *p*-states, *e.g.*, fig. 2. For multicomponent oxides we find that even at the bottom of the conduction band, *i.e.*, at the Γ point, the contributions from the oxygen *p*-states are significant, table 1. Thus, the key feature of the conduction band in a conventional TCO —its high energy dispersion— originates in a strong interaction between the cation *s*-states and the anion antibonding *p*-states [17]. The direct *s*-*s* overlap is insignificant, fig. 1, and therefore, the *s*-*s* interactions, which were commonly assumed to play to key role in the electronic properties of TCO [12,14,16], do not govern the transport properties in these oxides. Indeed, the small electron effective mass in s^2-cation oxides is determined by the strong *s*-*p* interactions [25].

From orbital symmetry considerations, one can see that the oxygen coordination *of cations* does not affect the *s*-*p* overlap. Instead, the largest overlap should be attained in materials where the oxygen atom is coordinated octahedrally *by cations* with the extended *s*-orbitals [17]. Our systematic comparison of the calculated electron effective mass in the oxides of metals with s^2 electronic configuration, fig. 4, shows that the mass slightly decreases as the ionic radii of the cations from the same group or the symmetry of the same-cation oxide increases. However, variations in the oxygen coordination as well as strong distortions in the metal-oxygen chains in different oxide phases lead to insignificant changes in the effective mass. For example, for cubic (octahedral coordination) and hexagonal (tetrahedral) ZnO or for corundum (distorted tetrahedral) and monoclinic β-phase (both distorted tetrahedral and trigonal) Ga_2O_3 the corresponding electron effective masses vary by 15% or 9%, respectively. The largest deviation in the effective mass values for various SiO_2 phases is 26%. Furthermore, the effective mass remains isotropic for all phases of the s^2-cation oxides —including silica ITQ-4 zeolite with large pore channels[1]. These observations explain the success of amorphous transparent conducting oxides —in marked contrast to the amorphous Si, where the directional interactions between the conduction *p*-orbitals lead to strong anisotropy of the transport properties which are sensitive to the orbital overlap and hence to the distortions in the atomic chains [14]. Finally, we note that the fact that the calculated as well as the observed [26] isotropic

[1]One exception is SiO_2 in high-temperature rutile phase with two unique Si-O bonds: the calculated effective mass in the *ab*-plane (long Si-O bond) is 2.6 times larger than the one in the *z*-direction (short Si-O bond).

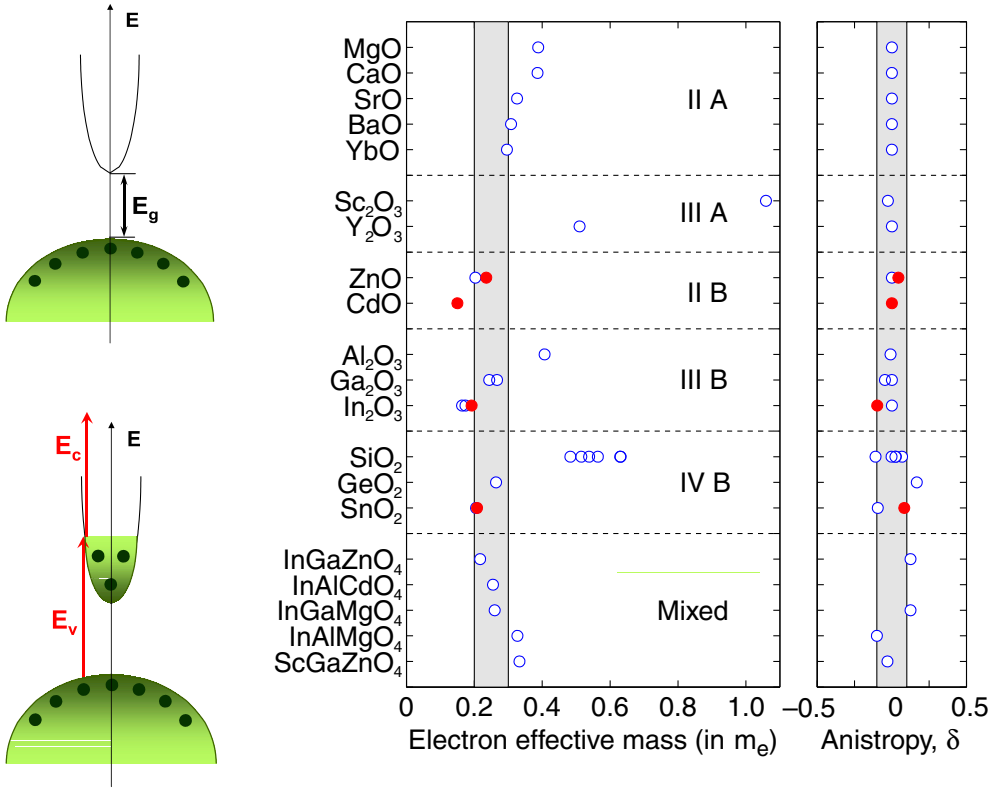

Fig. 4: (Colour online) The key electronic features of n-type TCO hosts. High energy dispersion of the conduction band (left) is essential for both high mobility of extra carriers due to their small effective mass and low optical absorption. For complete transparency in the visible range, the inter-band transitions E_v and E_c should be >3.1 eV, while the intra-band transitions as well as plasma frequency should be <1.8 eV. Such a dispersed conduction band along with the above-visible optical transitions at the Γ point are found in a variety of oxides with s^2-cation(s). The electron effective mass calculated for different oxide phases shows little dependence on the oxygen coordination and is isotropic ($\delta=(m_a+m_b)/2m_c-1$). The highlighted areas are to guide the eye; red circles represent currently known TCO hosts.

effective mass in rutile SnO_2 where the direct overlap between Sn s-orbitals is possible (only) along the [001] direction, corroborate our conclusion that the s-s interactions do not govern the transport properties as discussed above.

Effective mass averaging. – Because the local symmetry (nearest neighbors), the cation-oxygen bond lengths and, hence, the s-p overlap are similar in the single and multi-cation oxides, the intrinsic transport properties in the layered materials should be related to those in the single-cation oxides. Moreover, due to the hybrid nature of the conduction states in the multicomponent oxides, the states of all cations should give the same order of magnitude contributions to the effective mass. Thus, we expect the latter to be an "effective" average over the effective masses of the corresponding single-cation oxides. Indeed, we find that in case of one-dimensional atomic chain where two types of metal atoms alternate with oxygen atoms, the effective mass averaging can be derived analytically, fig. 3(f).

We formulate a simple approach which allows one to estimate the effective mass of the multicomponent oxides as follows. With proper doping, the Fermi energy is shifted up into the conduction band (Burstein-Moss shift). When the extra electrons propagate along the z-direction, *i.e.*, across the layers, the resulting resistivity is a sum of the resistivities of each layer. Therefore, the z-component of the average effective-mass tensor can be found as

$$m_z = (m_1 + m_2 + m_3)/3, \tag{1}$$

where $m_{1,2,3}$ are the effective masses of the corresponding single-metal oxides —In_2O_3, Ga_2O_3 and ZnO in the case of $InGaZnO_4$.

For the in-plane charge transport in the layered materials, the effective-mass tensor components can be found in a parallel fashion. Note, that one needs to average the effective mass for the mixed $GaZnO_{2.5}$ layers:

$$\frac{1}{m_{a,b}} = \frac{1}{3}\left(\frac{1}{m_1} + \frac{2}{\frac{1}{2}(m_2+m_3)}\right). \tag{2}$$

The resulting $m_{a,b}$ and m_z are presented in table 1. We find that the increase of the electron effective masses in the order $InGaZnO_4$ < $InAlCdO_4$ < $InGaMgO_4$ < $InAlMgO_4$ < $ScGaZnO_4$ is well reproduced by the above averaging.

Moreover, the $m_{a,b}$ and m_z values nearly coincide with the corresponding effective masses of the multi-cation oxides with the exception of the Sc case. In fact, for the Sc-containing compounds the effective mass averaging is not legitimate due to the presence of the empty d-states of Sc near the conduction band edge. In Sc_2O_3, the Sc d-states are located at 0.5 eV above the conduction band edge, and therefore give significant contributions to the effective mass which is about the mass of an electron. In the multi-cation oxide, the Sc d-states are found to be at $\sim$2 eV above the conduction band edge, so that the resulting small effective mass, table 1, is determined primarily by the s-p interactions —similar to the rest of the s^2-cation oxides.

The effective mass averaging procedure, eqs. (1) and (2), can be generalized for materials consisting of any number of layers, *e.g.*, for $InGaO_3(ZnO)_m$, m = integer. Furthermore, since the intrinsic transport properties are determined entirely by the local symmetry, *i.e.*, the nearest neighbors, the effective mass averaging should apply to TCOs in the amorphous state. In this case, one needs to average the components of the effective-mass tensor, $m_{amorph} = (m_a + m_b + m_z)/3$.

Importance of carrier generation. – Upon doping of a TCO host material, the resulting conductivity depends not only on the effective mass but also on the carrier generation mechanism, carrier concentration and carrier relaxation time. Doping of a structurally anisotropic material may lead to non-uniform distribution of the carrier donors and, therefore, the isotropic behavior of the host may not be maintained as, for example, in oxygen-deficient β-Ga_2O_3 [27]. In multicomponent $InGaO_3(ZnO)_m$, different valence states (In^{3+} and Ga^{3+} vs Zn^{2+}) and oxygen coordination (octahedral for In *vs.* tetrahedral for Ga and Zn) are likely to result in preferential arrangement of aliovalent substitutional dopants or oxygen vacancies. Consequently, an anisotropic mobility should be expected in the layered materials due to the spatial separation of the carrier donors and the layers where the extra carriers are transfered efficiently, *i.e.*, without charge scattering on the impurities. While targeted doping can help to make either or both structurally distinct layers conducting, the amorphous complex oxides readily offer a way to maintain isotropic transport properties. Indeed, experimental observations that the mobility and conductivity are independent of the large variations in the composition in amorphous $InGaO_3(ZnO)_n$ with $n \leqslant 4$ [12] and that the effective masses of amorphous and crystalline $InGaZnO_4$ are nearly the same [28] support our conclusions.

For efficient doping of wide-bandgap oxides such as MgO, CaO, SiO_2 and Al_2O_3, novel carrier generation mechanisms should be sought. A non-traditional approach has already yielded promising results in calcium aluminates [29–31] —a conceptually new class of transparent conductors [19]. Multicomponent oxides —such as those considered in this work, ordered ternary oxides [32] as well as their solid solutions and amorphous counterparts— represent an alternative way to utilize the abundant main-group elements such as Ca, Mg, Si and Al towards novel TCO hosts with a predictable effective mass and optical and transport properties controllable via the composition.

* * *

The work is supported by University of Missouri Research Board.

Appendix

Theoretical methods. – The first-principles full-potential linearized augmented plane wave method [33,34] with the local density approximation is employed for electronic band structure investigations of the XY_2O_4 compounds, X = In or Sc and Y = Ga, Zn, Al, Cd and/or Mg, and single-cation oxides. Cutoffs for the basis functions (16.0 Ry) and potential representation (81.0 Ry), and expansion in terms of spherical harmonics with $\ell \leqslant 8$ inside the muffin-tin spheres were used. The muffin-tin radii are 2.3 to 2.4 a.u. for In, Sc and Cd; 1.9 to 2.1 a.u. for Ga, Mg, Zn and Al; and 1.5 to 1.6 a.u. for O atoms. Summations over the Brillouin zone were carried out using at least 14 special **k** points in the irreducible wedge.

Structure optimization. – XY_2O_4 compounds have rhombohedral $R\bar{3}m$ crystal structure of $YbFe_2O_4$ type [35,36]. Indium (or scandium) atoms substitute Yb in 3(a) position, while both Y^{3+} and Y^{2+} atoms replace Fe in 6(c) position and are distributed randomly [37]. Our total energy calculations for several structures in the (a, $2a$,c) supercell with various arrangements of the Y^{2+} and Y^{3+} atoms suggest that their arrangement is not ordered but random —in agreement with the experiment. We note here that the electronic band structure features are similar for different spatial distributions of the Y atoms for the reasons discussed in the paper.

Since the valence state and ionic radii of Y^{2+} and Y^{3+} are different, the site positions of these atoms as well as their oxygen surrounding should be different. Because the exact internal positions of atoms are unknown, we used those of the $YbFe_2O_4$ [35] as the starting values and then optimized each structure via the total energy and atomic forces minimization. During the optimization, the lattice parameters were fixed at the experimental values [36,38]. We find that the optimized cation-anion distances correlate with ionic radii of the cations.

Single-cation oxides. – For the single-cation oxides, the following phases have been calculated: $Fm\bar{3}m$ for MgO, CaO, SrO, BaO and YbO; $Ia\bar{3}$ for Sc_2O_3 and Y_2O_3; $Fm\bar{3}m$ and $P6_3mc$ for ZnO; $Fm\bar{3}m$ for CdO; $R\bar{3}c$ for Al_2O_3; $R\bar{3}c$ and $C2/m$ for Ga_2O_3; $Ia\bar{3}$, $R\bar{3}c$ and $I2_13$ for In_2O_3; $P3_221$, $P2_1/c$, $P6_3/mmc$, $P4_12_12$ and $I2/m$ for SiO_2; $P4_12_12$ and $P4_2/mnm$ for GeO_2; $P4_2/mnm$ and $Pbcn$ for SnO_2. For each structure, the internal positions

of all atoms have been optimized via the total energy and atomic forces minimization, while the lattice parameters were fixed at the experimental values.

One-dimensional model of complex oxides. – The effective mass averaging, cf. eq. (1), can be shown analytically using a one-dimensional model in the tight-binding approximation. To capture the key features of complex oxides, we consider a chain consisting of two types of metal atoms which alternate with oxygen atoms, fig. 3(f), and assume only the nearest-neighbor interactions given by the hopping integrals β_1 and β_2. The Hamiltonian of this model system is

$$H = \sum_{n,l} |n,l\rangle \varepsilon_l \langle n,l| + \sum_{n,n',l,l'} |n',l'\rangle \beta_l \langle n,l|. \qquad \text{(A.1)}$$

Here, l is the atom index in the unit cell, n enumerates the cells and n', l' in the second sum run over the nearest neighbors. For the bottom of the conduction band, the dispersion relation can be simplified to

$$\varepsilon(k) = \frac{\varepsilon_1 + \varepsilon_2}{2} + \frac{1}{\frac{1}{2}(\frac{\Delta}{\beta_1^2} + \frac{\Delta}{\beta_2^2})} [ka]^2 \ , \qquad \text{(A.2)}$$

if $|\varepsilon_1 - \varepsilon_2| < 2 \left| \frac{\beta_1^2 - \beta_2^2}{\Delta} \right|$. Here ε_0, ε_1 and ε_2 are the atomic level energies of the oxygen and two types of metal atoms, respectively, and it is assumed that $\varepsilon_0 < \varepsilon_{1,2}$ and $\varepsilon_1 \sim \varepsilon_2$; $\Delta = \frac{1}{2}(\varepsilon_1 + \varepsilon_2) - \varepsilon_0$ and a is a half of the lattice parameter. Similar considerations for the chain consisting of only one type of metal atoms alternating with oxygen atoms show that the quantity $\frac{\Delta}{\beta^2}$ represents the effective mass of the system. Therefore, eq. (A.2) represents the effective mass averaging over those of the corresponding single-metal "oxide" chains, cf., fig. 3(f) —in agreement with the results of our first-principles calculations. The following parameters were used to plot fig. 3(f): $\varepsilon_0 = 1.00$, $\varepsilon_1 = 2.00$, $\varepsilon_2 = 2.05$, $\beta_1 = 0.4$ and $\beta_2 = 0.5$.

REFERENCES

[1] Chopra K. L., Major S. and Pandya D. K., *Thin Solid Films*, **102** (1983) 1.
[2] Thomas G., *Nature*, **389** (1997) 907.
[3] Ginley D. S. and Bright C. (Editors), Special issue on Transparent Conducting Oxides, *MRS Bull.*, **25** (2000).
[4] Ohta H. and Hosono H., *Mater. Today*, **7** (2004) 42.
[5] Edwards P. P., Porch A., Jones M. O., Morgan D. V. and Perks R. M., *Dalton Trans.*, **19** (2004) 2995.
[6] Neumark G. F., *Mater. Sci. Eng. R*, **21** (1997) 1.
[7] Van de Walle C. G., *Phys. Status Solidi B*, **229** (2002) 221.
[8] Zunger A., *Appl. Phys. Lett.*, **83** (2003) 57.
[9] Freeman A. J., Poeppelmeier K. R., Mason T. O., Chang R. P. H. and Marks T. J., *MRS Bull.*, **25** (2000) 45.
[10] Orita M., Takeuchi M., Sakai H. and Tanji H., *Jpn. J. Appl. Phys.*, **34** (1995) L1550.
[11] Orita M., Tanji H., Mizuno M., Adachi H. and Tanaka I., *Phys. Rev. B*, **61** (2000) 1811.
[12] Orita M., Ohta H., Hirano M., Narushima S. and Hosono H., *Phil. Mag. B*, **81** (2001) 501.
[13] Nomura K., Ohta H., Ueda K., Kamiya T., Hirano M. and Hosono H., *Science*, **300** (2003) 1269.
[14] Nomura K., Ohta H., Takagi A., Kamiya T., Hirano M. and Hosono H., *Nature*, **432** (2004) 488.
[15] Shannon R. D., Gillson J. L. and Bouchard R. J., *J. Phys. Chem. Solids*, **38** (1977) 877.
[16] Kawazoe H., Ueda N., Un'no H., Omata T., Hosono H. and Tanoue H., *J. Appl. Phys.*, **76** (1994) 7935.
[17] Mizoguchi H. and Woodward P. M., *Chem. Mater.*, **16** (2004) 5233.
[18] Ingram B. J., Gonzalez G. B., Kammler D. R., Bertoni M. I. and Mason T. O., *J. Electroceram.*, **13** (2004) 167.
[19] Medvedeva J. E. and Freeman A. J., *Europhys. Lett.*, **69** (2005) 583.
[20] Mryasov O. N. and Freeman A. J., *Phys. Rev. B*, **64** (2001) 233111.
[21] Asahi R., Wang A., Babcock J. R., Edleman N. L., Metz A. W., Lane M. A., Dravid V. P., Kannewurf C. R., Freeman A. J. and Marks T. J., *Thin Solid Films*, **411** (2002) 101.
[22] Yang Y., Jin S., Medvedeva J. E., Ireland J. R., Metz A. W., Ni J., Hersam M. C., Freeman A. J. and Marks T. J., *J. Am. Chem. Soc.*, **127** (2005) 8796.
[23] Medvedeva J. E., *Phys. Rev. Lett.*, **97** (2006) 086401.
[24] Medvedeva J. E., *Unconventional approaches to combine optical transparency with electrical conductivity*, (2007) arXiv:0704.1494.
[25] Kittel C., *Introduction to Solid State Physics* (John Wiley and Sons, Inc.) 2005, Chapt. 9.
[26] Button K. J., Fonstad D. G. and Dreybradt W., *Phys. Rev. B*, **4** (1971) 4539.
[27] Yamaga M., Villora E. G., Shimamura K., Ichinose N. and Honda M., *Phys. Rev. B*, **68** (2003) 155207.
[28] Takagi A., Nomura K., Ohta H., Yanagi H., Kamiya T., Hirano M. and Hosono H., *Thin Solid Films*, **486** (2005) 38.
[29] Hayashi K., Matsuishi S., Kamiya T., Hirano M. and Hosono H., *Nature*, **419** (2002) 462.
[30] Matsuishi S., Toda Y., Miyakawa M., Hayashi K., Kamiya T., Hirano M., Tanaka T. and Hosono H., *Science*, **301** (2003) 626.
[31] Medvedeva J. E., Freeman A. J., Bertoni M. I. and Mason T. O., *Phys. Rev. Lett.*, **93** (2004) 16408.
[32] Minami T., *J. Vac. Sci. Technol. A*, **17** (1999) 1765.
[33] Wimmer E., Krakauer H., Weinert M. and Freeman A. J., *Phys. Rev. B*, **24** (1981) 864.
[34] Weinert M., Wimmer E. and Freeman A. J., *Phys. Rev. B*, **26** (1982) 4571.
[35] Kato K., Kawada I., Kimizuka N. and Katsura T., *Z. Kristallogr.*, **141** (1975) 314.
[36] Kimizuka N. and Mohri T., *J. Solid State Chem.*, **60** (1985) 382.
[37] Li C., Bando Y., Nakamura M. and Kimizuka M., *J. Electron Microsc.*, **46** (1997) 119.
[38] Kimizuka N. and Mohri T., *J. Solid State Chem.*, **78** (1989) 98.